STIGMATICALLY FOCUSING PARTIAL PRESSURE ANALYZER WITH DUAL CHAMBER ION SOURCE

IN-35
100,022
47P.

Klaus F. Rasskopf

Translation of "Stigmatisch fokussierender Partialdruckanalysator mit Zweikammerionenquille", Technical University of Munich, Munich West Germany, 1971, pp. 1-43 (A72-22318)

(NASA-TT-20059) STIGMATICALLY FOCUSING PARTIAL PRESSURE ANALYZER WITH DUAL CHAMBER ION SOURCE Ph.D. Thesis - Technical Univ. of Munich, 1971 (NASA) 47 p Avail: NTIS HC A03/MF A01 N87-29800

CSCL 14B G5/35 Unclas 0100022

NATIONAL AERONAUTICS AND SPACE ADMINISTRATION
WASHINGTON, D.C. 20546 SEPTEMBER, 1987

STANDARD TITLE PAGE

1. Report No.	2. Government Accession No.	3. Recipient's Catalog No.
NASA TT-20059		

4. Title and Subtitle	5. Report Date
STIGMATICALLY FOCUSING PARTIAL PRESSURE ANALYZER WITH DUAL CHAMBER ION SOURCE	September 1987
	6. Performing Organization Code

7. Author(s)	8. Performing Organization Report No.
Klaus F. Rasskopf	10. Work Unit No.
	11. Contract or Grant No. NASW-4006

9. Performing Organization Name and Address	13. Type of Report and Period Covered
The Corporate Word, Inc. 3 Gateway Ctr., 18 S. Pittsburgh, PA 15222	Translation

12. Sponsoring Agency Name and Address	14. Sponsoring Agency Code
National Aeronautics and Space Administration Washington, DC 20546	

15. Supplementary Notes

Translation of "Stigmatisch fokussierender Partialdruck-analysator mit Zweikammerionenquelle," Technical University of Munich, Munich, West Germany, 1971, pp. 1-43.

A72-22318

16. Abstract

The partial pressure analyzer developed has a high absolute sensitivity and high resolution. Interaction effects, as they occur in conventional partial pressure analyzers between the heating filament for the emission of electrons and the residual gas, are suppressed by removing the heating filament from the measurement area. The electron beam is generated in an auxiliary vacuum compartment, and passes subsequently through an aperture into the ionization compartment. The probability is, therefore, small that the presence of substances produced at the heating filament by chemical reactions and thermal decompositions will have disturbing effects. The high sensitivity and resolution of the instrument are obtained with the aid of an electron path configuration of unconventional characteristics.

17. Key Words (Selected by Author(s))	18. Distribution Statement
	Unlimited

19. Security Classif. (of this report)	20. Security Classif. (of this page)	21. No. of Pages	22. Price
Unclassified	Unclassified	47	

NASA-HQ

TABLE OF CONTENTS

/5

1.	INTRODUCTION	4
2.	PROBLEMS OF PARTIAL PRESSURE ANALYSIS	4
2.1	Interaction free ion emitter	4
2.2	Dual chamber technique	5
2.3	Sensitivity and resolution	5
2.4	Transmission	6
3.	DESCRIPTION OF THE EQUIPMENT	7
	3.1. Magnetic field	7
	3.2. Dual chamber ion source	8
4.	CHARACTERISTICS OF OPERATION	10
	4.1. Resolution	11
	4.2. Resolution-limiting factors	11
	4.3. Sensitivity in the dual-chamber technique	13
	4.4. Experimental operation	14
	4.5. Dependency of operational characteristics on various parameters	16
	4.6. Single chamber operation	18
	4.7. Angle deflection of the ion beam	21
	4.8. Calibrating sensitivity	23
	4.9. Comparison with other residual gas analyzers	23
5.	DUAL CHAMBER TECHNIQUE	25
6.	POSSIBLE APPLICATIONS	28
7.	DISCUSSION	29
8.	APPENDICES	30
	8.1. Theoretical appendix (ion optics)	30
	8.2. Technical appendix	35
	8.2.1. Dual chamber arrangement	35
	8.2.2. Chamber evacuation and the vacuum system	35
	8.2.3. Magnet	36
	8.2.4. Ion emitter	38
	8.2.5. Photosensor	40
	BIBLIOGRAPHY	45

STIGMATICALLY FOCUSING PARTIAL PRESSURE ANALYZER WITH DUAL CHAMBER ION SOURCE

Klaus F. Rakopf

1. INTRODUCTION /1*

Advances in vacuum technology have made it possible to work in smaller and smaller pressures. In some applications it is absolutely necessary to know the composition of the residual gas in addition to the total pressure.

A number of commercial residual gas analyzers with good resolution and high sensitivity exist to meet this need. Generally speaking, however, they do not allow for the quantitative analyses of all the residual gas components because the composition of the residual gas is effected by the heating element. Of particular interest, therefore, are those instruments that allow unadulterated partial pressure analysis and, although they are small in size, have adequate sensitivity for measuring low partial pressure (10^{-10} Torr).

2. PROBLEMS IN PARTIAL PRESSURE ANALYSIS /2

2.1. Interaction free ion emitter

A residual analysis proceeds in three stages. First, the molecules of the gas are ionized in a vacuum by an electron beam; they are then divided according to their masses; and finally a graph of the relative frequencies of each mass provides a mass spectrum. The production of ions poses one of the greatest problems in the residual gas analysis process because, while in operation, the heating element strongly influences the composition of the residual gas. Thermal decompositions at the hot cathode produce fragments of the residual gas molecules. They are generally strongly reactive and produce new gaseous products either with other gases or on the container wall. In addition, the composition of the gas is altered by the (chemical) pump effect of the heating filament [1]. Therefore, the ion emitter does not operate free of interactions, which severely impedes exact measurement of the partial pressure. There are two possible methods for avoiding these disruptive effects. The heating filament can be eliminated and ions produced by a process other than thermal emission, or the attempt can be made to suppress the undesirable effects of the hot cathode.

---

*Numbers in the margin indicate pagination in the foreign text.

There are several possible alternatives to thermal emission, some of which are mentioned below.

Cold cathodes are already being used to measure total pressure [2,3,4]. However, their disadvantages (nonlinearity and instability at higher currents) do not allow for satisfactory results.

A cold cathode emitter was recently developed [5] that delivered stable currents of 0.1...0.2 mA (milliangstroms). Its operating temperature did not significantly exceed 20°C. Its use in ultra high vacuums, however, presented problems such as heat capacity, etc. Other adverse indications were the wide distribution of energy and the early behavior of the equipment at start-up.

Another possible method for producing ions might be field ionization. However, the current is too low for partial pressure measurement in ultra high vacuums, and it requires extremely high voltages. Field ionization is practical only in specialized cases.

Higher electron currents could be achieved through the use of a secondary electron multiplier [7]; but this becomes too expensive for a residual gas analyzer.

In exceptional cases, electron production is possible by photoionization.

P. Schagen, in a comprehensive 1965 study of alternatives to thermal emission, credits p-n-layer emitters with the best chance of replacing the hot cathodes. Currents are given at mA/cm^2. But here, too, development is incomplete.

If thermal production of electrons is desirable, using the lowest possible operating temperature can reduce the influence of the heating filament. Cathode materials with a low electron affinity should be used (thoriated tungsten or rhenium wires). The operating temperature of the heating filament can be lowered further by decreasing the electron current. However, the ion emitter must then be extremely efficient. Satisfactory results were obtained with magnetron ion emitters (electron current: some 10^{-8}) [9,10].

2.2 Dual chamber technique

The partial pressure analyzer developed here employs a totally different method for blocking the undesirable effects of the hot cathodes; the "dual chamber technique" proposed by E.W. Blauth [11]. It does not require elimination of thermal electron production, but it significantly diminishes its negative characteristics by removing the heating element from the actual measurement area. The heating element sits in an auxiliary vacuum compartment and shoots electrons through a narrow aperture into the

measurement area. There is therefore only a small probability that substances produced by chemical reactions at the cathode will reach the measurement area and be detected.

2.3 Sensitivity and Resolution /3

An additional problem in residual gas analyses is obtaining the highest possible sensitivity with satisfactory resolution--a prerequisite for partial pressure measurement in ultra high vacuum (UHV).

The greatest sensitivity can be obtained through the use of ion sources with a large ionization volume because the sensitivity (A/Torr) of the partial pressure instrument at a given pressure and electron current is proportional to the volume present.

2.4 Transmission

The production of intensive ion currents in electron impact ion emitters is limited for several reasons as indicated above; thus, great attention must be paid to transmission problems during partial pressure measurement [12]. Optimal conformation of the ion source and separation system is essential because sensitivity is proportional to the product of the spectrometer transmission and the efficiency of the ion source.

The narrow inlet opening (s_E<0.5 mm) normally used in static mass spectrometers to increase resolution significantly reduces the transmission of such instruments. Spectrometer transmission is usually 1 to 10% [13]. Therefore, a desirable separation system would require no inlet opening and could completely process an extracted ion beam of wide diameter, thus showing high total transmission.

In order to make high sensitivity possible, various commercial instruments (Varian PPG, Vams; see Table 2) operate with the acceleration field strongly penetrating the ionization area, so that a volume with a larger cross section (as compared to the inlet opening) can be used. However, the electron paths to the extraction field must be reduced to a narrow space, otherwise the energy distribution needed for resolution will be too broad. But even with this method, total transmission cannot be raised above 10% (spectrometer transmission is greater, of course, with these very efficient instruments).

Stigmatically focusing the electron beam is highly advantageous for obtaining high sensitivity. "Stigmatic" means focusing radially as well as axially. This will allow detection even of those ions whose paths do not run parallel to the apparatus' plane of symmetry (xy-plane in Fig. 14). These ions are lost when a purely cylindrical lens (without axial focusing) is used because, in the narrow space between the magnet's pole pieces,

they impinge against the chamber's wall or against the pole pieces themselves.

The demands for a) an interaction free emitter
b) large ionization volumes
c) high transmission (wider inlet opening)
d) stigmatic image
e) good resolution ability

absolutely must be satisfied simultaneously.

An apparatus that satisfies demands c), d), and e) is the panoramic spectrometer of Weissmann [14] (staggered entry and exit of the ions, field borders logarithmically curved, partial stigmatic focusing). Another apparatus was proposed by Smythe et al. [44] (circular boundaries to the pole pieces, parallel electron beams, no inlet opening, transmission circa 12%). A leak detector was developed according to the same concept in 1948 by Stein [9] in which the ions are produced in a large volume source according to the magnetron principle.

3. DESCRIPTION OF THE EQUIPMENT /4

3.1. Magnetic Field

This apparatus makes it possible to satisfy simultaneously the demands for stigmatic focusing, high transmission, and a large volume ion source by using a particular magnetic separating system which is distinguished by its simplicity. A nonhomogeneous magnetic field is produced between flat but inclined pole pieces, whose slope is 1/r, whereby r begins at the intersecting lines of the pole piece surfaces (Fig. 1). The theory of the movement of charged particles in such a field was first considered by Richardson [15]. This field design was applied to mass spectrometry by Poschenrieder and Warnect [16] and Liebl [17].

Such a field has the following characteristics:

It stigmatically draws an incident parallel ion beam by diverting 90° and being under certain geometric restrictions. moreover, since (as will be shown) dispersion is independent from site δ of the shot (Fig. 1), the inlet opening can be dispensed with, which means that an entire (cylindrical) ion beam of substantial diameter (approx. 10 mm) can penetrate the magnetic field without the aperture causing loss of intensity.

The nonhomogeneous magnetic field used in this apparatus makes it possible to combine a static separating system (full resolution) with an ion source, which can process large ionization volumes. Viewed optically, a volume element, which can be quite large due to the reduction associated with focusing, is shown in infinity.

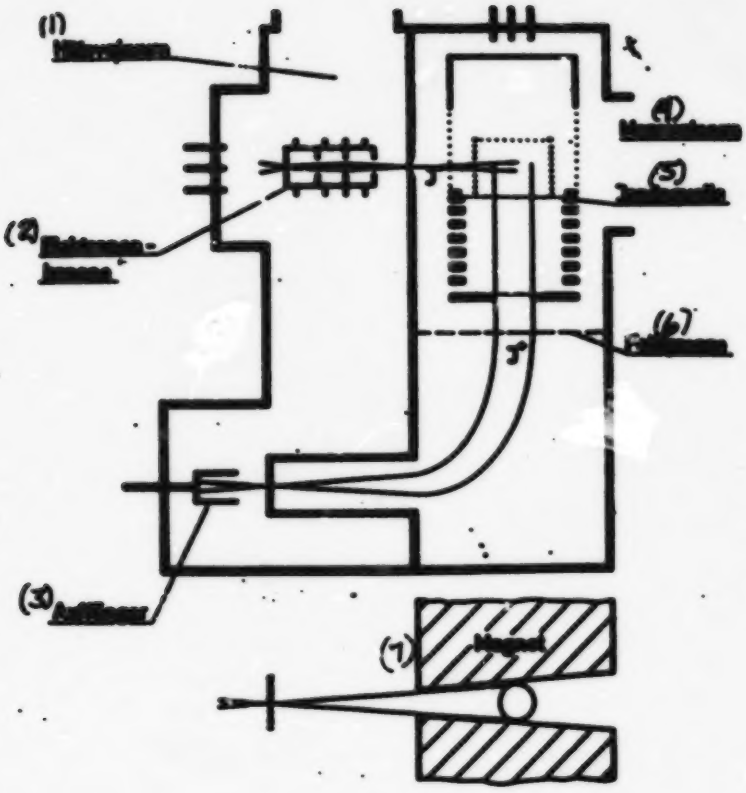

Fig. 1. Drawing of the partial pressure analyzer

Key: (1) Auxiliary vacuum; (2) Electron gun; (3) Collector; (4) Measuring vacuum; (5) Ion emitter; (6) Field boundaries; (7) Magnet.

3.2. Dual Chamber Ion Source /5

The choice of separating system necessitated construction of an ion emitter suited to the specific characteristics of this field's configuration. The emitter was to produce a parallel ion beam, on which strict quality requirements were imposed as regards angle and energy dispersion. (See 4.7.) Moreover, since the source operates on the dual chamber principle, construction is not simple (Fig. 2).

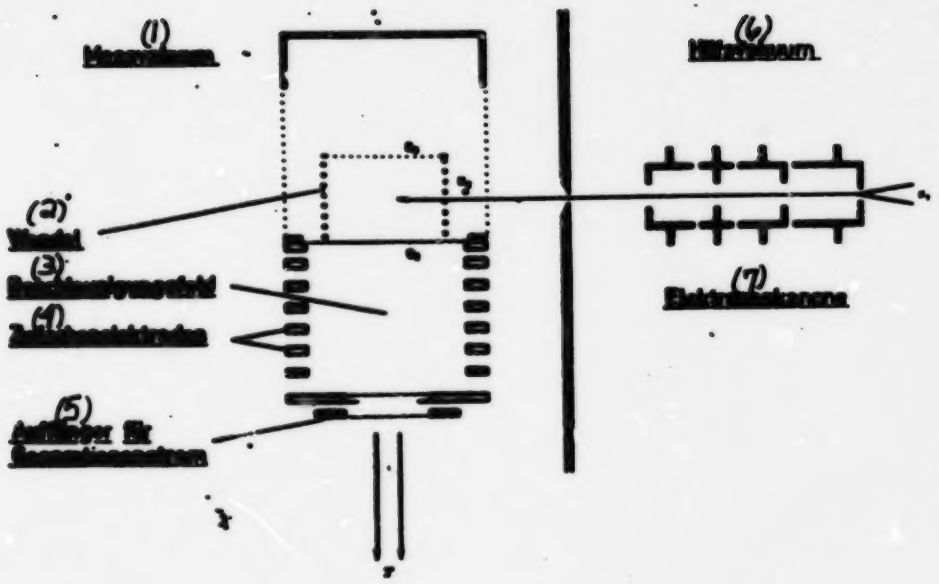

Fig. 2. Dual chamber ion emitter.

Key: (1) Measuring vacuum; (2) Coil; (3) Acceleration field; (4) Intermediate electrodes; (5) Collection for total ion current; (6) Vacuum; (7) Electron gun.

In a dual chamber ion emitter, electrons are produced by an electron emitter placed in an auxiliary vacuum compartment (see 3.2.4.). The beam is shot after the electrons have passed at low molecular current through an aperture between the auxiliary and main vacuum chambers.

The ionization compartment is surrounded by a wire coil W and two fine mesh screens (G_2 and G_B). A constant low voltage at the coil produces a homogeneous axial electrical field, which drives the ions, formed by electrical impulses in the ionization area, through gate G_2. The ions are accelerated between gates G_2 and G_1, which are exactly parallel to each other and have high transmission. Using gates in the inlet and outlet apertures of the acceleration compartment and attaching intermediate electrodes R, which are at equidistant potentials, guarantee uniformity of the accelerated field, so that the ions leave the emitter as parallel beams (uniform field accelerator [18,19]).

The resistance of the coil was chosen to ensure that the temperature reached during operation is high enough to avoid adsorption of gases, which could be redesorbed, but not so high that gas replacement reactions occur.

To make possible a direct comparison between normal (single chamber) operation and the dual chamber operation, a second filament K_2 was installed inside the ion emitter.

Moreover, the electric current supplied by K_2 can be substantially increased to measure the highest sensitivity of the design (single chamber operation).

After being diverted in the magnetic field, the ion beam leaves the measuring vacuum through a short outlet and is detected by a Faraday collector, which is located in the same auxiliary vacuum compartment as the electron gun (Fig. 1).

4. CHARACTERISTICS OF OPERATION /6

Several factors are important in the evaluation of a mass spectrometer and its applicability to special cases, the most important being resolution and sensitivity. Resolution is the ability of the device to different neighboring mass lines (measured for the most part in 10% valley resolutions and half resolutions). Sensitivity in A/Torr indicates the size of the ion flow relative to pressure; to compare efficiency, ion flow is measured relative to pressure and electron flow in $Torr^{-1}$. [20]

Also important are mass area, pressure area, the lowest detectable partial pressure and partial pressure sensitivity (=lowest detectable partial pressure/total pressure).

Resolution and sensitivity have opposite tendencies relative to the most important parameters (ΔU, θ_1) and the product of the two can be used as a standard for a rough comparison of various devices.

Resolution and sensitivity are dependent upon various parameters in a complex way:

efficiency of the ion emitter
ion beam quality (energy and angle dispersion)
transmission
required resolution capacity
width of outlet aperture
grid composition
geometry (refraction radius).

4.1 Resolution

The anticipated resolution is determined basically by the variation in energy ΔU and the angle dispersion Θ_1 of ion beam. The reason for the variation in energy is that the ions can originate along the potential gradients prevalent in the coil, while angle dispersion Θ_1 is due to dispersion at the acceleration grids and the thermal energy of the ions.

The equation (see 8.1.) for mass dispersion is

$$y = 1{,}085 \cdot A_0 \cdot \frac{\Delta M}{M} \tag{1}$$

and for theoretical resolution (half value),

$$A_{th} = \frac{M}{\Delta M} = \frac{1}{2{,}828 + 1{,}414\,\Theta_1} \cdot \tag{2}$$

Taking s_A, the width of the outlet aperture, into account one arrives at the actual resolution,

$$A_p = \frac{M}{\Delta M} = \frac{1{,}085 \cdot A_0}{(2{,}828 + 1{,}414 \cdot \Theta_1) \cdot 1{,}085\, A_0 + s_A} \tag{3}$$

(A_0 is a geometric factor).

In addition to the dependency of resolution on the width of the outlet aperture and energy variation ΔU, the strong influence of angle deflection (linear) is also noteworthy. Thus, in this magnetic field configuration high demands are placed on the parallelism of the ion beam. However, the use of an inlet aperture here is superfluous.

4.2 Resolution limiting factors

The lack of energy definition ΔU is determined by the volume of the electrons. The ions are generated along the coil's dominant potential gradients of about 7 volts/cm, so that the energy corresponding to the diameter of the electron beam is approximately 1 volt. Since the electrons may pass through the coil several times and are not magnetically conducted, the actual lack of energy definition is at 2 to 3 volts. /7

The potential of grid G_1 also influences ΔU. At higher positive voltage, G_1 acts as a counterfield, i.e., it does not allow ions to pass if their energy is too low, and thereby produces a decrease in ΔU.

Two additional components also contribute to the lack of angle definition Θ_1. As the ions accelerate through grids G_1 and G_2, a lack of angle definition α_1 is produced in addition to the lack of energy definition ΔU_2. According to [21], it can be estimated at

$$\alpha_1 = 2 \cdot \alpha_{Streu} = \frac{0.4}{z \cdot d} \qquad (4)$$

Key: Streu = scattering, deflection

where z is the number of grid crosspieces per mm, and d is the distance between the two nets.

The finer the mesh, the lower the dispersion (but also the transmission).

The second component arises from the fact that the ions already in the ionization chamber contain a transversal energy component E_t (thermal energy, charges, nonhomogeneities in the field of stress, penetration of external potentials through the coil, increased energy of the ions during dissociative ionization) and enter even below an angle of α_2 in the acceleration field (Fig. 3). Because $v = \sqrt{2E/m}$, this angle decreases on acceleration only by the fact $w = \sqrt{E_t/E_{Be}}$ ab (E_{Be} = acceleration energy). Therefore, θ_1 is already 3.6^0 at an E_t of 0.5 volts. When the thermal energy of the ions is $E_t = 0.025$, then $\theta_1 = 0.4^0$.

These limiting factors must naturally be seen in conjunction with achievable sensitivity

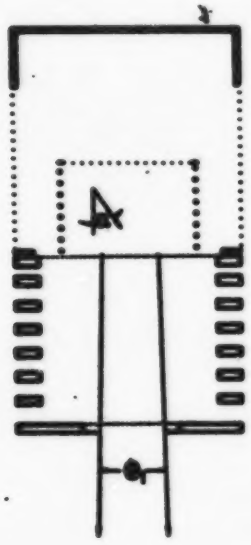

Fig. 3: Angle deflection of the ion beam.

Of course, these resolution limiting factors must be seen in relation to the attainable sensitivity. Thus, for example, the use

of fine mesh grids does not really improve resolution because the grid effects (ΔU_2) are small even at a mesh width of 0.11 mm as compared with the influence of the thermal energy (θ_1). Transmission would drop, however.

Screens of larger mesh have greater transmission, of course, (up to 97%) and improve the efficiency of the ion source, but the beam characteristics (ΔU, θ_1) drop rapidly as mesh widths increase so that transmission drops. Higher sensitivity is impossible despite the greater ion source efficiency. Grids with a mesh of 0.11 mm and optical transmission of 78% have proven optimal.

Where the two grids are separated by 25 mm, they $\alpha_{streu} = 0.05^{o}$, according to equation (4).

Where these grids are used, the maximum possible half value resolution ($s_A = 0$, $\Delta U = 0$) is

$$A_{0,5} = \frac{1}{\Delta U/U + 1{,}44 \cdot \theta_1} = \frac{1}{1{,}44\,(\alpha_1 + \theta_{Therm.})} = 85 \qquad (5)$$

Only grid effects and thermal energy were considered here, as opposed to the energy and angle deflection created by the potential gradients in the ionization chamber. Allowing for lack of definition $\Delta U_1 = 2$ volts (assumed), the maximum expected resolution becomes $(A_{0.5})_{max} = 65$.

4.3. Sensitivity in the dual chamber technique /8

The yield of the ion source is actually limited as the following applies to electron collision ion sources:

$$J^{+} = J^{-} \cdot p \cdot s \cdot l \text{ bzw.} \quad E = J^{+} : p = J^{-} \cdot s \cdot l \approx 8 \cdot 10^{-4} \text{ A/Torr.} \qquad (6)$$

(J^{+} = ion beam, J^{-} = electron beam, p = pressure, s = differential ionization, l = length of path)

It appeared that (to maintain the resolution demanded) the potential of G_2 had to be set so high that only about 40% of the ions produced could leave the source. The remaining ions are reflected onto G_2 because of their greater energy and angle deflection. Taking grid transmission into consideration, the following results for the beam leaving the source:

$$E = 2 \cdot 10^{-4} \frac{A}{Torr}$$

(measured at G_A).

The measured sensitivity is $E = 10^{-4}$A/Torr, which yields $T_{sp} = 50\%$ for spectrometer transmission. This higher value is made possible by the special field geometry since no entry aperture is necessary to lower intensity.

Despite the loss during passage through G_2 (see above), the total transmission E_G of the device (=ions recorded/ions produced) is remarkably high at about 12%.

4.4 Experimental Operation

The values achieved (A, E,...) have been compiled in Table 1. It shows that nearly maximum resolution was attained while sensitivity at 10^{-4} A/Torr, or 1.2 $Torr^{-1}$, was very high. That indicates that the angle deflection of the beam, which basically determines resolution, does not exceed the size given by thermal and grid effects. The cause of widening mass lines 1, 12, 14, and 16 lies in the considerable energy of the fragmentary ions which originated at dissociation (also see Table 3; cracking patterns).

TABLE 1

		Zwei-kammer-betrieb	Ein-kammer-betrieb
(1)	Theoretische Auflösung (Halbwerts-)	65	
(2)	Experimentelle Auflösung		
	Halbwerts-	60...70	30
	10 % Tal-	28	15
(3)	Partialdruckempfindlichkeit		
	in A/Torr	10^{-4}	10^{-2}
	in $Torr^{-1}$	1,2	1,4
(4)	Gesamtdruckempfindlichkeit		
	in A/Torr		$5 \cdot 10^{-2}$
(5)	Spektrometertransmission (%)	50	20
	Total Gesamttransmission (%)	12	15
(6)	Elektronenstrom (mA)	0,08	7,5
(7)	Elektronenenergie (V)	100	250

Key: (1) Theoretical resolution (half value); (2) Experimental resolution (half value - 10% valley); (3) Partial pressure sensitivity in A/Torr, in $Torr^{-1}$; (4) Total pressure sensitivity in A/Torr; (5) Spectrometer transmission (%); (6) Electron beam (mA); (7) Electron energy.

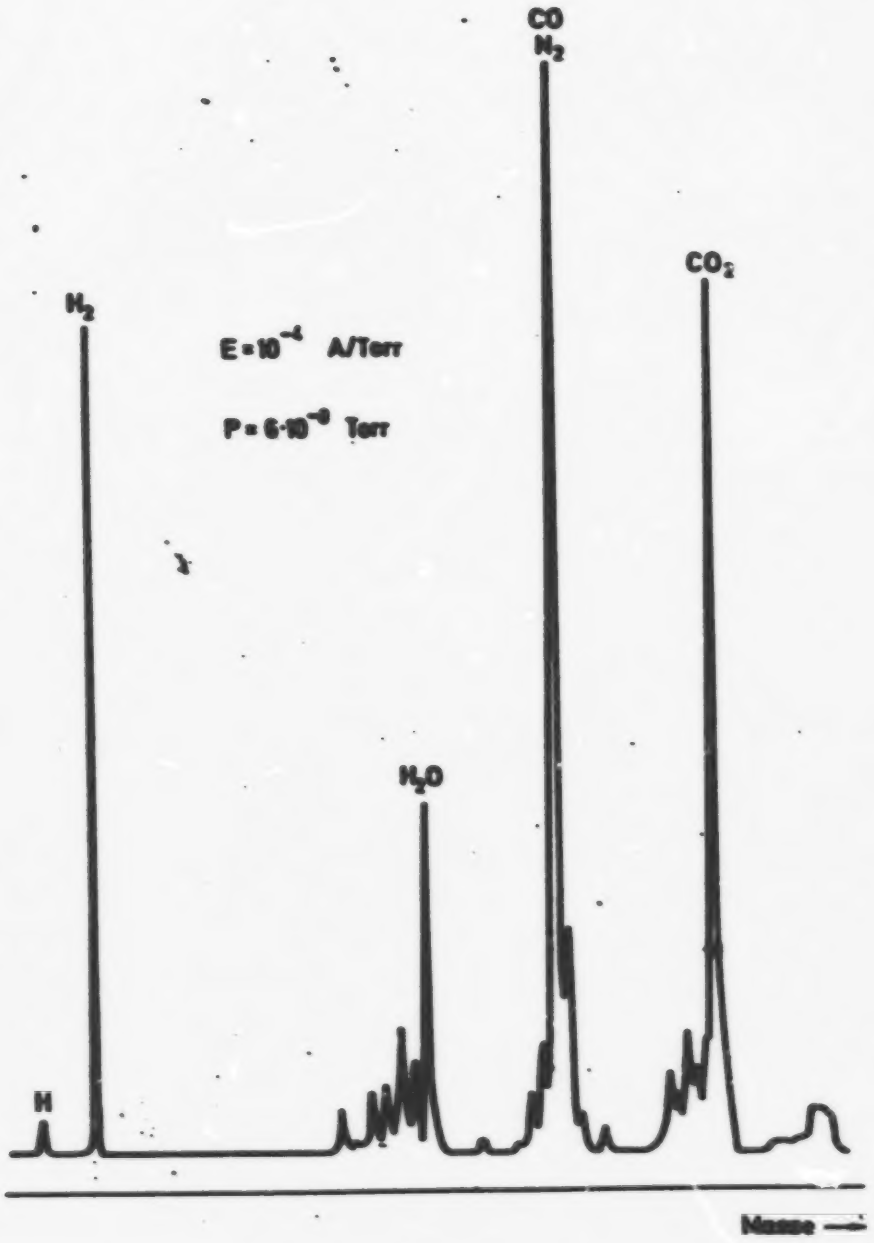

Fig. 4. Residual gas spectrum (Dual chamber technique)

Key: Masse = volume

4.5 Dependency of operational characteristics on various parameters /10

Dependency on the potential of grid G_2 (U_{Be}).

Since the potential of grid G_2 demonstrated the most significant influence on the yields obtained, resolution and sensitivity were measured dependent upon U_{G2} (for the dual chamber operation) and shown graphically in Fig. 5. It is obvious that the device operates optimally at U_{Be} = 512 volts, because the product of $A_{0.5} \cdot E_p$ reaches a maximum at this value. Resolution is worse at rising or falling grid tensions because of the increasing nonhomogeneity of the tension field (Fig. 10).

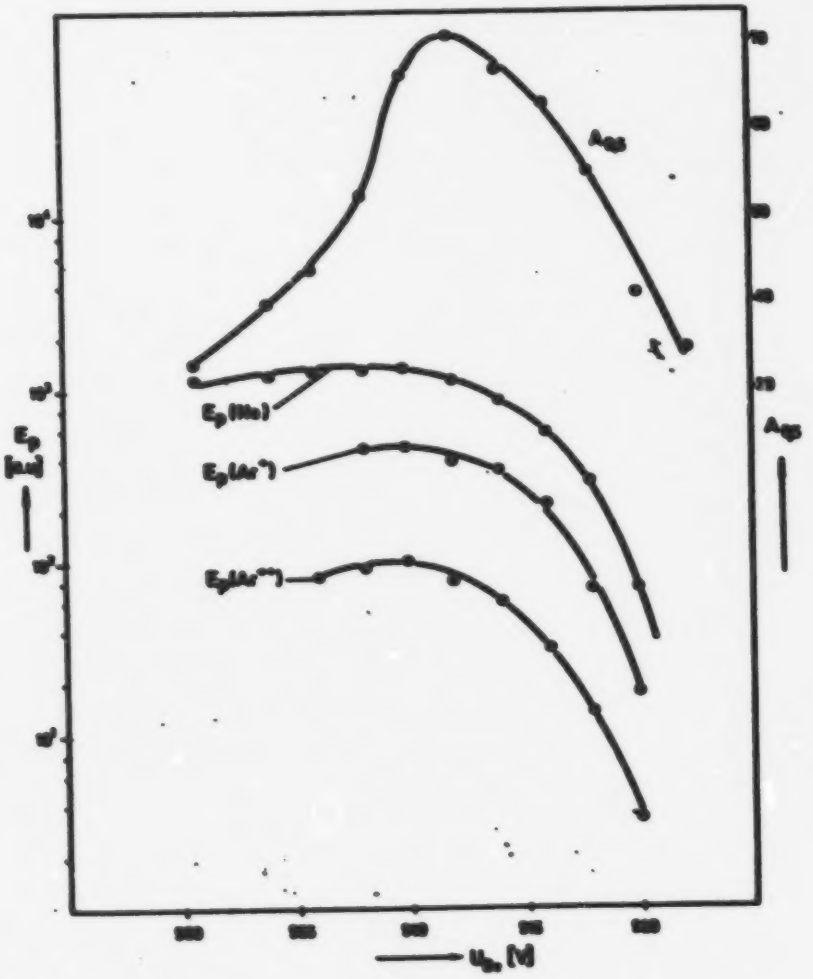

Fig. 5: Dependency of partial pressure sensitivity Ep and half-value resolution $A_{0.5}$ on the potential of grid G_2 (U_{Be}).

Linearity /11

The dependency of partial pressure sensitivity on the pressure was measured over six ten-day periods for both the single and dual chamber operations, and is shown graphically in Fig. 6. Linearity is guaranteed for pressures of up to some 10^{-5} Torr.

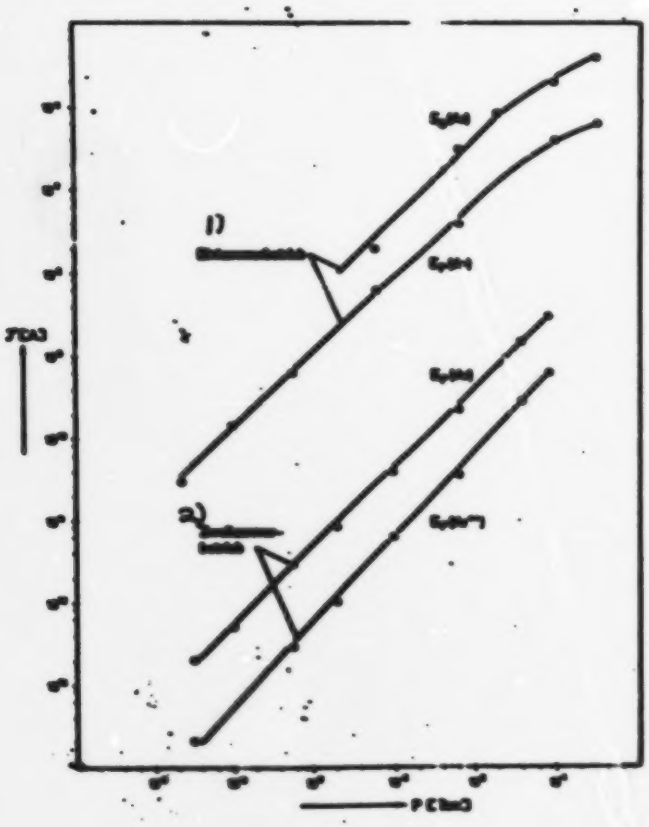

Fig. 6: Linearity of partial and total pressure sensitivities Ep and E_G, respectively.

Key: 1) Single chamber operation; (2) Dual chamber operation.

As Fig. 7 infers, the ratio of ion beam J^+ to electron beam J^- is constant only in the case of the smaller electron beam. The initial volume charge effect appears in the sharp rise in the curve beginning $J^- > 50$ μA. According to [22], the potential troughs created by the electron volume charge reach 0.1 Ev ($E_{thermal}$) where, for example J^- = 50 μA, beam diameter is approx 1 mm, and electron energy of 100 volts. Therefore, the ions are captured and last longer in the potential troughs [23,24,25]. Because of the greater likelihood of being hit frequently by electrons, cracking patterns change as the volume charge (or stopping time) increases, i.e., more fragmentary ions appear [45]. Thus, at J^- = 100 μA, the ratio J^+_{H2O}/J^+_{H2O} = 0.28 (Fig. 4) rather than 0.25 (see Table 3). This volume charge effect is somewhat reduced by the established field of stress. /12

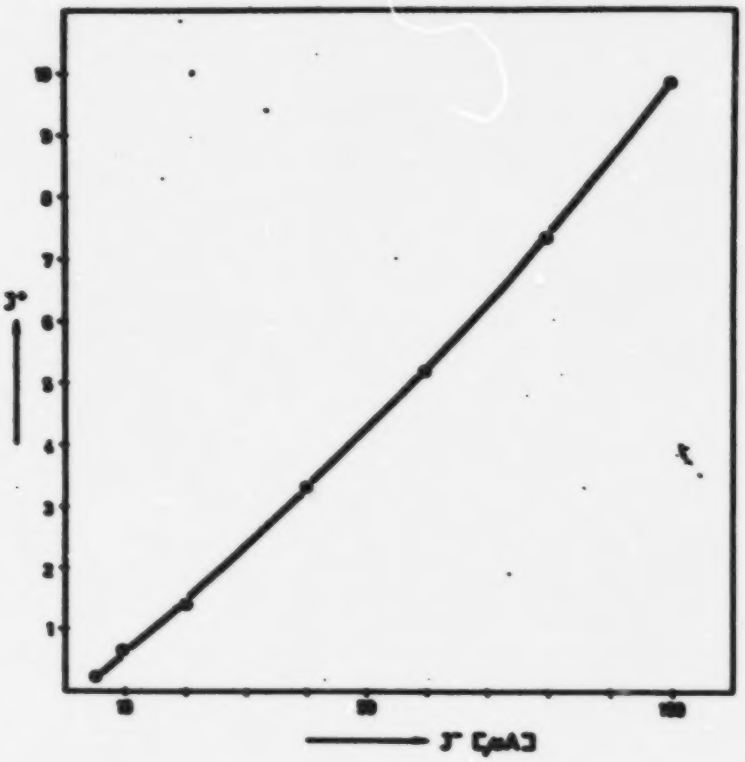

Fig. 7: Relationship of ion beam J^+ to electron beam J^-.

4.6 Single chamber operation

The following resolution limiting factors appear during operation of the auxiliary heating filament directly adjacent to the coil (not a dual chamber operation).

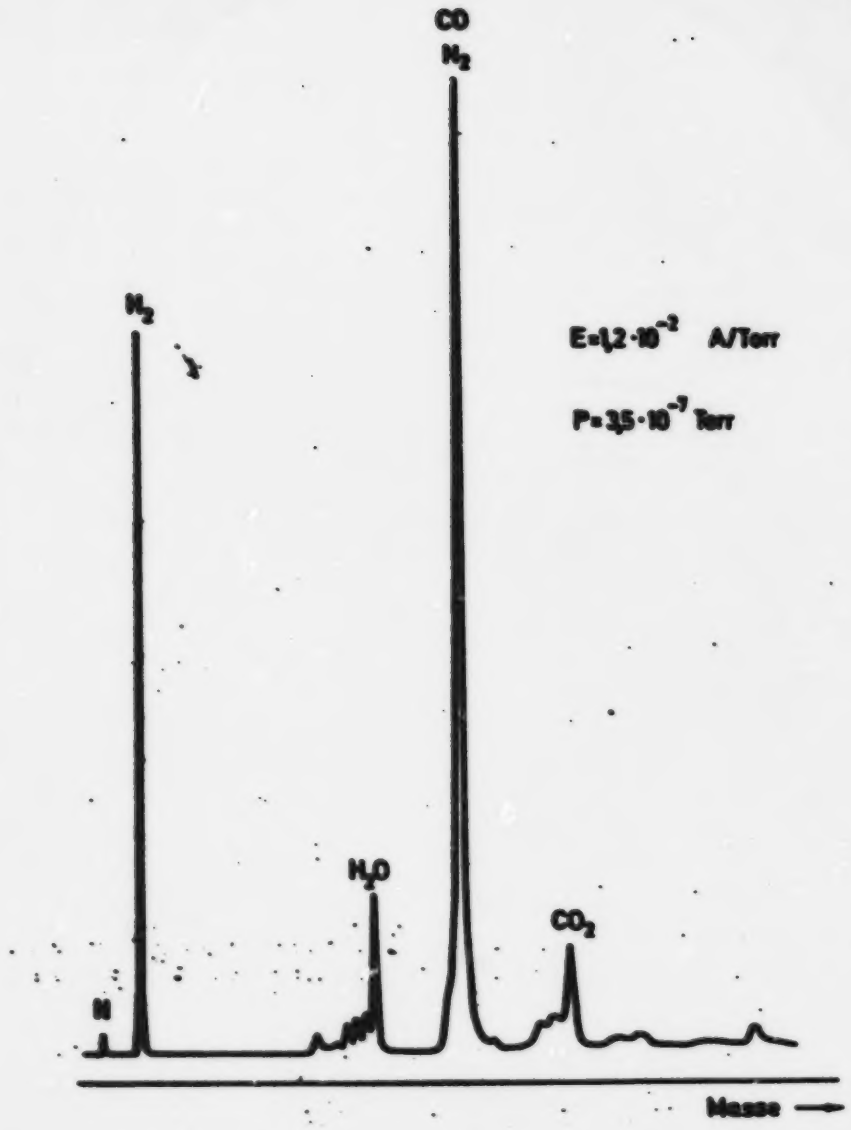

Fig. 8: Residual gas spectrum (single chamber operation).

The electron beam is increased to 7.5 mA. To overcome the volume charge forces generated by the high electron density, the electron energy was raised to 230 volts. That leads to a drop in the differential ionization of a factor of 1.3 [26]. On the basis of the altered potential ratios, the electrons oscillate several times in the coil so that yield increases as a result of the longer electron path.

It is very difficult, and not very important, to calculate resolution because of the volume charge. This is because the resolution attained in single chamber operation and the best dual chamber results are attained in an identical apparatus. Adjustment errors are likewise negligible. /13

Fig. 8 shows a spectrum with the highest sensitivity. Fig. 9a includes a portion of the spectrum shown in 9b with $2 \cdot 10^5$ times higher sensitivity. Partial pressures below $2 \cdot 10^{-13}$ Torr can be detected.

/14

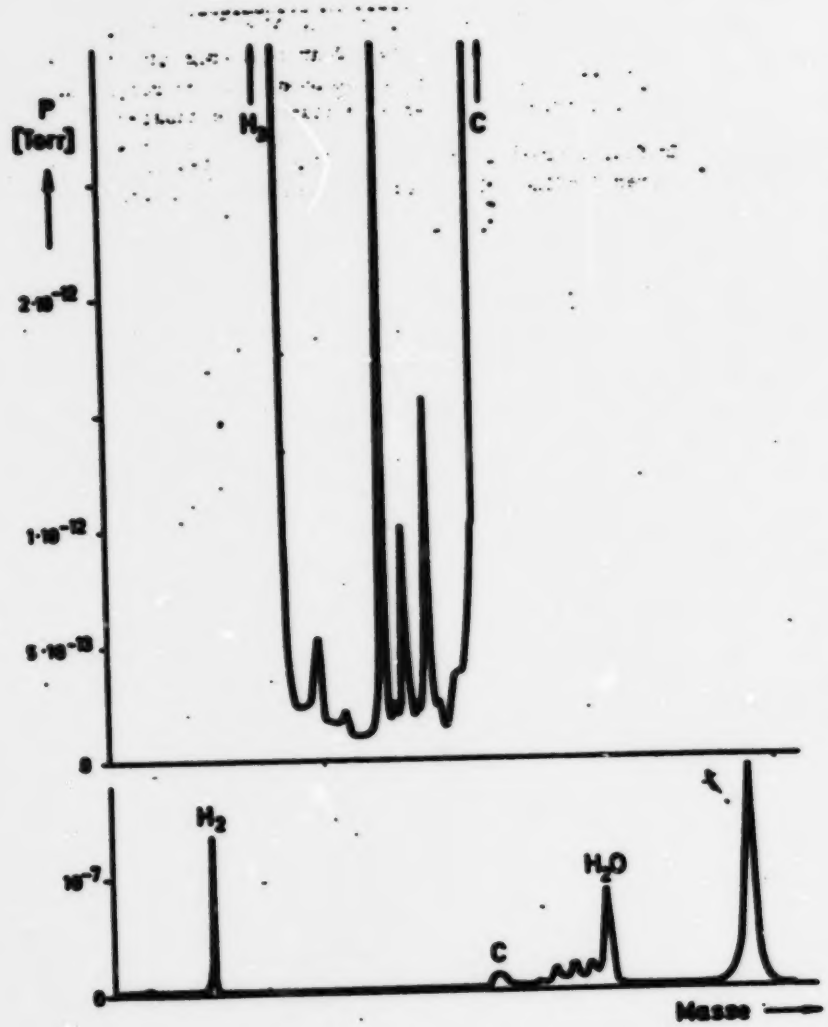

Fig. 9: a) Residual gas spectrum with high sensitivity (above)
b) Residual gas spectrum with low sensitivity (below)

Expansion of the volume charge in the ion beam

At high pressure and high J- the perveance of the beam is so great that the expansion of the volume charge in the beam limits transmission. At perveances below 10^{-8} A/V$^{3/2}$ these effects are negligible [27].

In the case of the largest beams of approx. 10 μA measured in the Mimas, the perveance (U=500 volts; argon) is:

$$P = \frac{J}{U^{3/2}} \sqrt{\frac{m_{Ion}}{m_{Elektron}}} = 2{,}5 \cdot 10^{-7} \frac{A}{V^{3/2}}$$

The measurements confirm the decrease in transmission expected with increasing pressure ($P>10^{-6}$Torr). Thus, Fig. 6 clearly shows that the ratio of the beam at curves b and a drops as pressure increases (J_b^+/J_a^+ = transmission).

The distribution of ions on the residual gas molecules /15
likewise causes a loss in transmission at higher pressures ($>10^{-5}$). According to [28], this can be approximated by the following formula:

$$J = J_0 \cdot \exp\left(-\frac{x \cdot d}{\lambda_0}\right) \quad \text{wo} \quad \begin{matrix} \lambda_0/\text{Torr} = \text{freie Weglänge} \\ \text{und } d = \text{Laufstrecke} \end{matrix}$$

Key: (1) where; (2) unlimited path length; (3) distance.

E.g., $J = 0.76 \cdot J_0$ for argon at 10^{-4} Torr and 30 cm distance.

4.7. Angle deflection of the ion beam

The strong dependency of resolution on angle deflection lends urgency to the capability of testing for parallelism of the ion beam alone. For this purpose an image sensor was constructed which transforms the ion beam into an electron beam after it passes through a filter screen and a drift field. The image of the filter screen thereby generated is projected onto a fluorescent screen and provides information about the angle deflection of the ion beam (description of the transformer in 8.2.5.)

Resolution and sensitivity can be strongly influenced by altering the tension at grid G_2 (Fig. 5). An examination of the ion beam with the image sensor shows that the angle scattering depends on grid tension UBe. It is lowest in dual chamber operation at U_{Be} = 511 volts: $\alpha<0.1^0$ (Fig. 11d). Resolution, therefore, has its maximum at this tension. Appropriate selection of the electrode tension achieves a highly homogenous tension field in the coil and permits extraction of the ions as a parallel beam (Fig. 10a).

Lowering U_{Be} creates a bending of the equipotential lines in the lower portion of the coil. The result is a focusing of the ion

beam, as seen in Fig. 11a and 11b. At the same time, the ion flow increases because the tension field is stronger and the ions are sucked out in greater volume. However, partial pressure sensitivity does not increase because transmission drops (the same is true for resolution).

If U_{Be} is increased, the equipotentials in the coil become distorted in such a way that the ion beam leaves the source divergently (Fig. 10c). The potential distribution has a saddle point. In the upper part, the field acts in a scattered and accelerated manner (due to the concavity of the potential lines); in the lower part, however, it is hesitant, but still scattered (convexity of the potential lines). The ion beam is divergent (Fig. 11e) and also less intense because of the counterfield effect of G_2.

The energy distribution of the ions is influenced by the tension U_{Be}. As tension rises, G_2 acts more and more like a counterfield, i.e., it lets only those ions through whose energy exceeds a specified value [29,30,31,32,33]. This improves the ground and thus also the partial pressure resolution. However, this effect is small compared to the influence of angle deflection because the deviation measured in Fig. 11 from the parallelism of the entire beam also qualitatively confirms the dependency of resolution on grid tension U_{Be} as shown in Fig. 5.

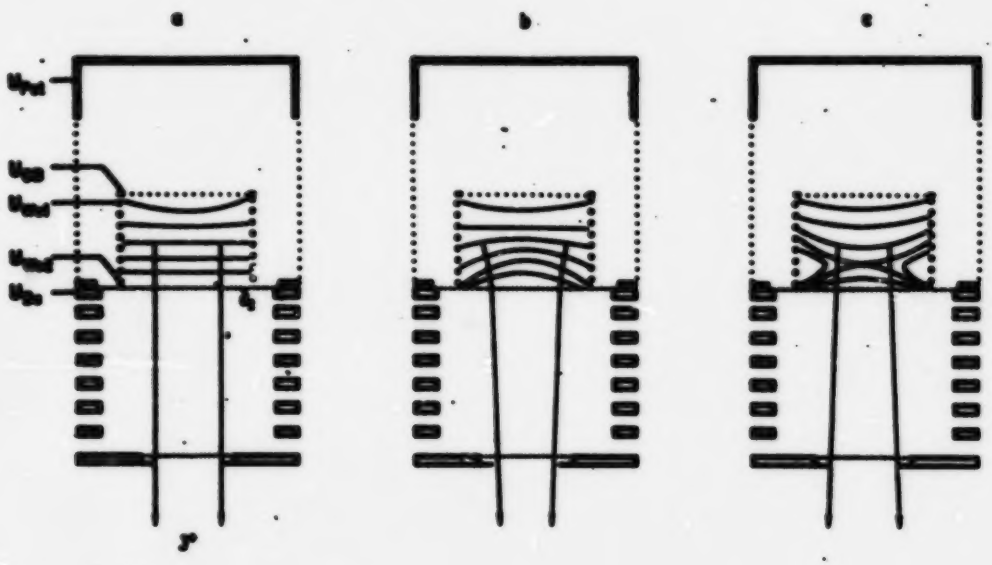

Fig. 10: Effect of grid potential U_{Be} on the parallelism of the beam.

ORIGINAL PAGE IS
OF POOR QUALITY

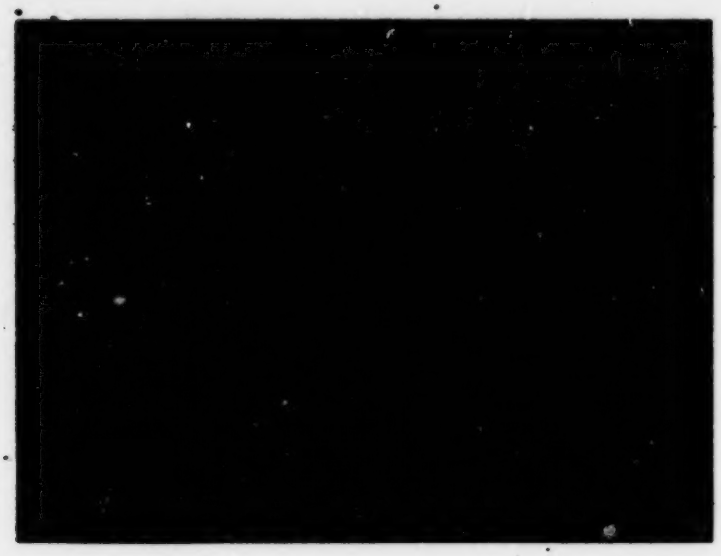

a). b) c) d) e)
(U_{Be} = 492 V) (500) (506) (511) (515)

Fig. 11: Beam deflection as dependent on grid potential U_{Be}.

4.8. Calibrating sensitivity /17

The spectrometer was not calibrated absolutely because this requires considerable expenditure. A Bayard-Alpert-Tube was used to measure pressure (nitrogen equivalent).

An indirect calibration results, however, from a comparison with the Varian (PPG) residual gas analyzer which was installed at the same location on the pump stand as the equipment developed here ("Mimas"). The sensitivity and resolution reported by Varian were confirmed (Table 2), therefore the sensitivity attained in the "Mimas" under nearly identical conditions (pressure, heating, geometric configuration, etc.) can be considered reliable.

4.9. Comparison with other residual gas analyzers

Table 2 [20] lists the details of some commercial partial pressure measuring devices. Among comparable static mass spectrometers (deviation radii were to be about equal), the device developed here assumes the indicated position as regards effectiveness (sensitivity in Torr-1).

The product of resolution times sensitivity can also be used as a criterion for judging a residual gas analyzer. A much higher value for that is attained in single chamber operation.

ORIGINAL PAGE IS
OF POOR QUALITY

TABLE 2: COMPARISON OF SOME PARTIAL PRESSURE ANALYZERS /18

Type of Instrument	Commercial Instr.	Mass Range (Mass Number)	Pressure Range (Torr)	Resolution (a)	Sensitivity (A $Torr^{-1}$)	Minimum detectable partial pressure (Torr)	Sensitivity x Resolution (A $Torr^{-1}$)	Sensitivity ($Torr^{-1}$)
180° Magnetic Deflection	GEC-AEI Vacuum MK10	2,3,4 12 to 200	10^{-3} to $5\cdot10^{-12}$	100	$5\cdot10^{-5}$	$5\cdot10^{-13}$	$50\cdot10^{-4}$	
	GEC-AEI Minimass	2,4 12 to 60 48 to 200	10^{-6} to 10^{-11}	unit mass separation up to 28		$1\cdot10^{-11}$		
	Edwards E 100	1,2,3,4 5 to 105	10^{-4} to 10^{-11}	44	$4\cdot10^{-5}$	$1\cdot10^{-10}$	$20\cdot10^{-4}$	0,3
	Vacuum Generators Micromass 1	2 to 240	10^{-2} to $3\cdot10^{-12}$	20	$3\cdot10^{-4}$	$3\cdot10^{-12}$	$60\cdot10^{-4}$	
	Vacuum Generators Micromass 2	2 to 240	10^{-2} to $3\cdot10^{-11}$	40	$3\cdot10^{-5}$	$3\cdot10^{-11}$	$12\cdot10^{-4}$	
90° Magnetic Deflection	Vacuum Generators Micromass 6	2 to 300	10^{-3} to 10^{-14}	150 (Multiplier)	100	$1\cdot10^{-14}$		
	Vans	1 to 110		45	10^{-3}	$5\cdot10^{-12}$	$450\cdot10^{-4}$	1
	Hiuac (Quadrupole)	1 to 200	10^{-3} to $3\cdot10^{-11}$	26	10^{-4}	$3\cdot10^{-11}$	$30\cdot10^{-4}$	1,2
	Hiuac (Normal operat.)	1 to 200	10^{-3} to $3\cdot10^{-13}$	25	10^{-2}	$3\cdot10^{-13}$	$1500\cdot10^{-4}$	1,4
90°/135° Magnetic Deflection	Varian Partial Pressure Gauge	1 to 70	10^{-3} to $2\cdot10^{-13}$	12	10^{-2}	$2\cdot10^{-11}$ $5\cdot10^{-13}$ (with external electrometer)	$1200\cdot10^{-4}$	1,5
60° Magnetic Deflection	Edwards E 60	1 to 25 2 to 50 12 to 200 25 to 350	10^{-3} to 10^{-14}	unit mass separation up to 200	$4\cdot10^{3}$ ($Torr^{-1}$) with multiplier	$1\cdot10^{-14}$		
Coincident-field cycloidal	Consolidated Electrodynamics 21-615	2 to 100	10^{-5} to 10^{-12}	unit mass separation up to 50	$5\cdot10^{-4}$	$2\cdot10^{-12}$		
	Consolidated Electrodynamics 21-614-1	2 to 11 12 to 200	10^{-4} to 10^{-12}	unit mass separation up to 150	$5\cdot10^{-5}$	$5\cdot10^{-11}$		
	Balzers QMG 60	1 to 100 2 to 200 2 to 300	10^{-3} to 10^{-12}	1 % definition 100	$2\cdot10^{-4}$	$2\cdot10^{-13}$		
	Ultek Magnetic Cycloidal	2 to 100	$2\cdot10^{-4}$ to $2\cdot10^{-11}$	30	10^{-3}	$5\cdot10^{-12}$		

5. DUAL CHAMBER TECHNIQUE /19

Chemically active gases (H_2, H_2O, CO_2, O_2 and hydrocarbons) create problems during the operation of mass spectrometers because they can dissociate at the surface of the hot cathode. The products of this dissociation are usually very reactive and react with other gases or surfaces. They produce new gaseous products and cause a notable change in gas composition [28].

Per [1], the following are possible reactions that might occur at the heating filament:

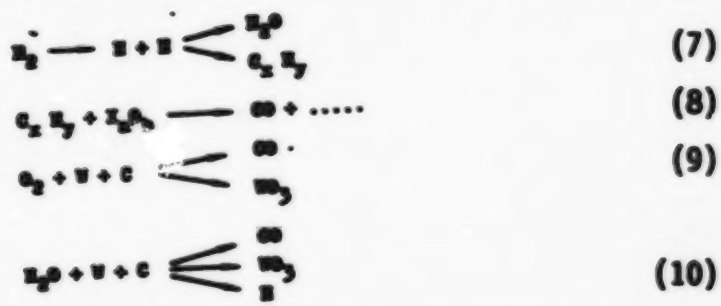

(7)

(8)

(9)

(10)

Above T = 1000°K, a significant amount of active hydrogen is produced at the heating coil by dissociation [34] but it is quickly absorbed on most of the surfaces (abnormally high pump velocity for H_2). Contamination layers (CO) occur during the interaction of H with the chamber wall and electrodes. They can cause a radical change of the residual gas spectrum [35]. CO_2 reacts to CO and O_2 at the heating filament [36]. Another undesirable effect of the heating filament is that the neighboring electrodes become warm from radiation. The cathode also emits charged and neutral particles and thereby contributes to the alteration of the residual gas (evolution of the gas).

These chemical and thermal effects can be reduced by using cathodes at lower operating temperatures only to a certain extent.

The "dual chamber technique" offers a significant improvement.

Comparison between dual chamber technique and normal operating procedures (single chamber technique).

This comparison considers the spectra in sequence and has the identical configuration as the ion emitter with open B.A. tubes.

The electrons were produced with K_1 (dual chamber) or K_2 (single chamber technique). To make an absolute comparison possible, inert gases (neon and argon) were introduced. If they are standardized to the same sensitivity, then the spectra in Figs. 12 and 13 result (total pressure: about 10^{-8} Torr).

As seen, the residual gas spectra differ markedly. The hydrogen dissociation occurring at the heating filament particularly changes the ratio H_1/H_2 (=0.240). The ratio caused solely by the electron impact dissociation per Table 3 is: H_1/H_2 = 0.008.

This value can be closely approximated by the dual chamber technique: H_1/H_2 = 0.032. The still too abundant atomic hydrogen seems to arise from the coil (electron impact desorption; hydrogen desorbes atomically [37]). /21

A clear rise in the CO partial pressure during the single chamber technique was expected since nearly all of the possible reactions described at the beginning of this chapter render CO.

The drop in the CO_2 partial pressure can likewise be ascribed to the effect of the heating filament ($CO_2 \xrightarrow{\text{Heating}} CO$). However, the build-up of CO and CO_2 is still not totally explained. It requires the presence of H_2O and/or O_2; the ratio of CO to CO_2 depends on the amount of H_2O and O_2.

/20

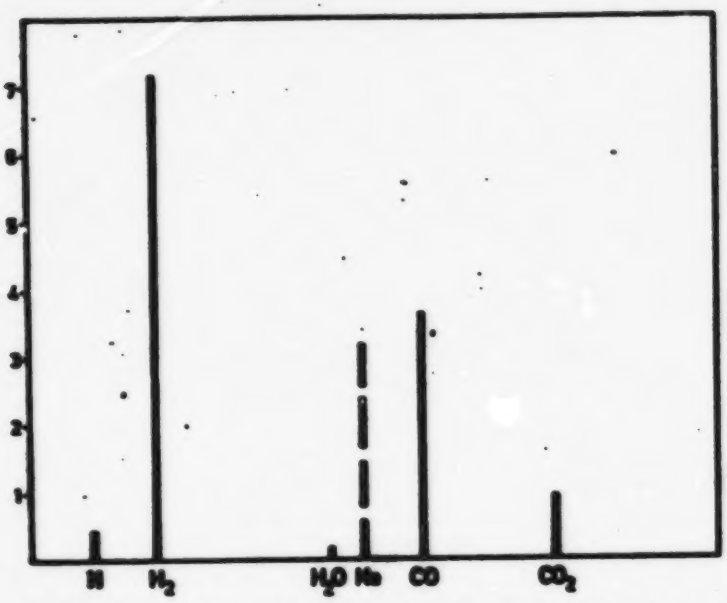

Fig. 12: Residual gas spectrum with dual chamber technique.

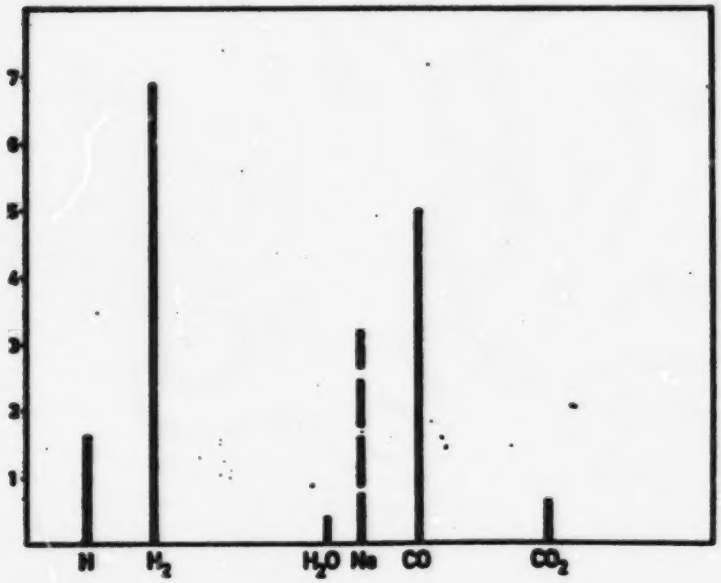

Fig. 13: Residual gas spectrum with single chamber technique

TABLE 3: TYPICAL "CRACKING PATTERN" DATA FOR RESIDUAL GAS ANALYZERS (PRIMARY PEAK INTENSITY = 100).

Gas	1	2	12	13	14	15	16	17	18	24	25	26	27	28	29	30	31	32	33	37	44
H_2	0·8	100	–	–	–	–	–	–	–	–	–	–	–	–	–	–	–	–	–	–	–
CH_4	1	2·4	2·1	4·8	11	80	100	–	–	–	–	–	–	–	–	–	–	–	–	–	–
NH_3	0·3	–	–	–	2·5	7·3	92	100	2·3	–	–	–	–	–	–	–	–	–	–	–	–
H_2O	6	2·2	–	–	–	–	2·3	25	100	–	–	–	–	–	–	–	–	–	–	–	–
N_2	–	–	–	–	5·5	–	–	–	–	–	–	–	–	100	–	–	–	–	–	–	–
CO	–	–	2	–	0·8	–	–	–	–	–	–	–	–	100	1	0·3	–	–	–	–	–
C_2H_6	0·4	1	0·3	0·5	1·3	2·7	0·3	–	–	0·7	3	19	30	100	21	26	0·6	–	–	–	–
O_2	–	–	–	–	–	–	7·1	–	–	–	–	–	–	–	–	–	–	100	–	–	–
Cl	–	–	–	–	–	–	–	–	–	–	–	–	–	–	–	–	–	–	100	30	–
CO_2	–	–	1·7	–	–	–	4·8	–	–	–	–	–	–	–	13	–	–	–	–	–	100

6. POSSIBLE APPLICATIONS /22

The many operations that are done with mass spectrometric methods in the field of physical-chemical research can be divided into various groups.

One part of this work attempts to clarify the phenomena created by electron impact. By measuring ionization and dissociation possibilities and appearance potentials, one can gain insight into ionization and dissociation mechanisms, chemical bonding forces and energy conditions of atoms, molecules and free radicals.

The dual chamber partial pressure analyzer developed here is particularly suitable for the quantitative analysis of light hydrocarbons because the very intensive interaction between heating filament (dissociation) and the gas composition is suppressed. This is highly significant in the research into the decomposition of molecules [60].

Another important application is the study of adsorption, condensation and electron impact desorptions. It is notable that most of the conventional partial and total pressure analyzers demonstrate quite different values (in extreme cases, factor 10) because a strong interaction occurs between the heating filament and impact field. The advantage of a PPA operating per the dual chamber technique to study electron impact desorption of chemically active gases (H_2, O_2, H_2O, CO, C_xH_y) by mass spectrometry is that there will be almost no products created at the heating filament, meaning that these gases are desorbed and produced at the filament simultaneously.

Little attention is given to this situation in much of the work being done on electron impact desorption [46...56] so that these measurements have a more qualitative character. Accurate control of the residual gas is often lacking as well.

It is not possible to eliminate the heating filament effect by a "zero measurement" because an interaction exists. Thus, e.g., the atomic hydrogen created at the heating filament through thermal dissociation [34] is quickly absorbed on the surrounding metal surfaces, thus also on the surfaces to be studied. This prohibits determination of its source during desorption by electron impact. This effect does not exist in the dual chamber partial pressure analyzer. It therefore makes possible quantitative measurements of the electron impact desorption (effect averages).

The high sensitivity (and transmission) of the device is advantageous for desorption studies because one can work with low electron currents (high currents would warm the target and thereby lead to thermal desorption).

Ions produced by the ionization of the residual gas can be partially inhibited by arranging counterfield configurations upon receipt of the collector [57, 58].

Partial pressure analyzers (PPAs) can also be used to examine special chemical reactions, i.e., to identify and measure reaction products and short-lived radicals, to clarify the reaction mechanism and reaction kinetic. An example would be the thermal decomposition of hydrocarbons [59]. A "dual chamber technique" (or a method with an equivalent effect) is indispensable in such cases to avoid the falsification of measurement results by the heating filament.

PPAs are used extensively in industry and research for control and supervision because of their high measuring sensitivity. Thus, e.g., the partial pressure of residual gas components must be suppressed during manufacture of semiconductor layers by vaporization as their build-up could cause undesirable changes in the film's properties.

Even more significant is knowing the partial pressures (particularly H_2) during film production by means of sputtering, since production depends heavily on hydrogen partial pressure.

Its high partial pressure sensitivity also makes it /23
possible to use the dual-chamber PPA for detecting leaks. Because of its advantages over convential PPAs (single chamber), it is also being considered with the motorized accelerator that is used in the field of surface physics (H^+ to 150 keV).

It should be reemphasized that the dual-chamber PPA concept has achieved a strong reduction of the effect of the PPA as an "active" element in the vacuum device. Previously, continual operation of conventional PPAs had not been possible during processes particularly sensitive to partial pressure since the change in the partial pressure and gas production by the heating filament could falsify measurements. This effect is far less detectible in the dual-chamber PPA because the operation of the device scarcely influences test conditions. These "passive" operational properties throw its field of application wide open.

7. DISCUSSION

A comparison between conventional (single chamber) operations and the dual-chamber method can show that the falsification of the residual gas composition caused by the heating filament was strongly reduced during partial pressure measurements despite the still existing connection between the two chambers. Therefore, it is also possible to measure quantitatively the partial pressure of reactive or slightly dissociating gases.

Its particular properties make the dual-chamber partial pressure analyzer particularly suited for a few additional applications in which conventional analyzers have been used with only limited success.

The favorable resolution and sensitivity values obtained by reason of the device's special ion optic concept are comparable to the values of commercial partial pressure analyzers.

I am grateful to Priv. Docent Dr. E.W. Blauth for the opportunity to carry out this work in the Institute for Plasma Physics. My special gratitude goes to Dr. H. Liebl, whose interest and support significantly contributed to my work. My thanks also goes to Dr. W. Poschenrieder for our many stimulating discussions. I would like to express my appreciation to Priv. Docent Dr. E. Konecny for kindly filling the role held by Priv. Docent Dr. E.W. Blauth following the latter's unexpected death.

8. APPENDIX

8.1 Theoretical Appendix

Fig. 14 shows the path of the ions in the nonhomogeneous magnetic field. The coordinate system of the magnetic field is z, r. The equation for the exit beam is given in xy coordinates.

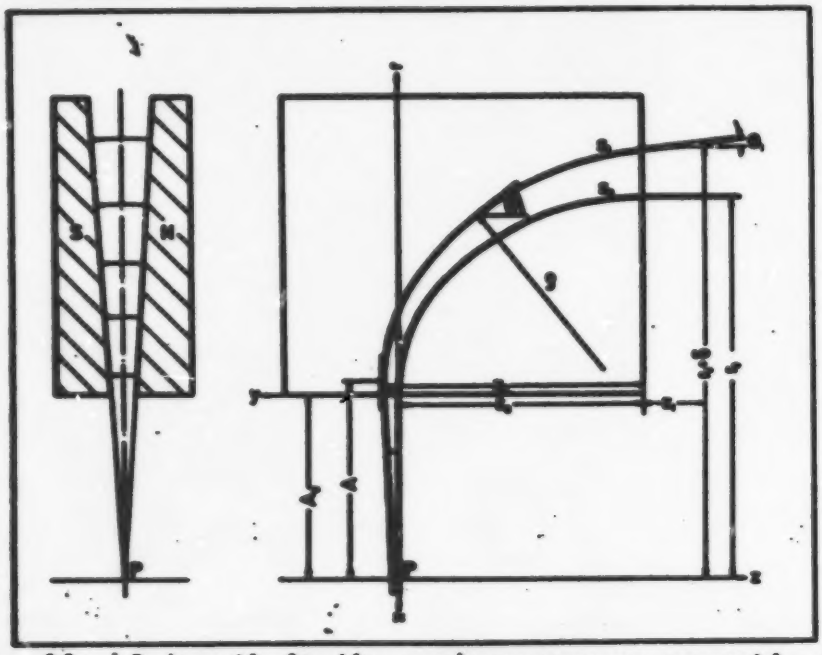

Fig. 14: Ion path in the nonhomogeneous magnetic field.

The tangential field strength in the wedge-shaped gap in the magnetic field is

$$B = \frac{\Phi}{y}. \tag{11}$$

The curve radius of the path of a charged particle is

$$\rho = \frac{p}{e \cdot B} = \frac{p \cdot r}{e \cdot \Phi} = K \cdot r. \tag{12}$$

The resolution of the movement equation for a particle path (parameter representation: 0) provides

$$r = A \cdot e^{K \cos \theta} \tag{13}$$

$$z = A \cdot K \cdot J(K, \theta) \tag{14}$$

whereby

$$J(K,\theta) = \int_0^{\theta} \cos \theta \cdot e^{K \cos \theta} \, d\theta \tag{15}$$

Determination of deflection requires the equation for the beam's exit path (after penetrating the magnetic field) dependent on the beam's entry parameters. /26

The incoming beam s1 is characterized by the following parameters.

Impulse width μ: $p = p_0 (1 + \mu) \qquad K = K_0 (1 + \mu)$ (16)
Angle deflection θ_1.
Shot site $r_0 + \delta$

The equation for the exit beam is (simplicity of half in xy system; originate in exit point of s_0 from the magnetic field)

$$y = z_2 - z_1 - z_0 - \alpha \cdot x \tag{18}$$

z_0, z_1, z_2, α must be determined dependent on δ, θ, μ.

From (5) follow:

$$z_2 = A \cdot K \cdot \int_0^{\pi/2 + \alpha} \cdot \cos\theta \cdot \exp(K \cdot \cos\theta) \, d\theta = A \cdot K \cdot J\left(K, \frac{\pi}{2} + \alpha\right) \tag{19}$$

$$z_1 = A \cdot K \cdot \int_0^{\theta_1} \cos\theta \exp(K \cdot \cos\theta) \, d\theta = A \cdot K \cdot J(K, \theta_1) \tag{20}$$

$$z_0 = A_0 \cdot K_0 \cdot \int_0^{\pi/2} \cos\theta \exp(K_0 \cdot \cos\theta) \, d\theta = A_0 K_0 C_0 \tag{21}$$

Calculation of α:

Entry:

$$\left.\begin{aligned} r &= r_0 + \delta \\ \theta &= \theta_1 \end{aligned}\right\} \text{in (12)}$$

$$r_0 + \delta = A \cdot e^{K \cos \theta_1} \quad . \tag{22}$$

Exit:

$$\left.\begin{aligned} r &= A_0 \\ \theta &= \frac{\pi}{2} + \alpha \end{aligned}\right\} \text{in (12)}$$

$$A_0 = A \cdot e^{K \cdot \cos\left(\frac{\pi}{2} + \alpha\right)} = A \, e^{-K \cdot \sin\alpha} \tag{23}$$

From (22): A determines $A = (r_0 + \delta) \cdot e^{-K \cos \theta_1}$

in (23): α determines

$$A = (r_0 + \delta) \cdot e^{-K \cos \theta_1} \cdot e^{-K \sin\alpha} = (r_0 + \delta) e^{-K (\cos \theta_1 + \sin \alpha)}$$

$$\alpha \approx \sin\alpha = \frac{1}{K_0 (1+\mu)} \cdot \ln \frac{r_0 + \delta}{A_0} - \cos \theta_1 = \frac{A_0}{K_0 r_0} \cdot \left(\frac{\delta}{A_0}\right) - \frac{A_0^2}{2 r_0 K_0} \cdot \left(\frac{\delta}{A_0}\right)^2 - \frac{A_0}{K_0 r_0} \cdot \left(\frac{\delta}{A_0}\right) \mu - \mu + \mu^2 + \frac{\theta_1^2}{2} \tag{24}$$

Calculation of z2 - z1 - z0 yields per H. Liebl [43]:

$$\begin{aligned} z_2 - z_1 - z_0 = A_0 K_0 \cdot \{ & (c_2 + c_0 - \tfrac{1}{K_0}) \cdot \mu - e^{K_0} \cdot \theta_1 + c_0 \cdot e^{-K_0} \left(\tfrac{\delta}{A_0}\right) + \\ & + (c_{22} + c_2 (1 - K_0) - \tfrac{1}{K_0}) \cdot \mu^2 + \tfrac{1}{2K_0} \cdot \theta_1^2 - e^{K_0} \cdot \theta_1 \cdot \mu - \theta_1 \cdot \left(\tfrac{\delta}{A_0}\right) + \\ & + e^{K_0} \cdot (c_2 + c_0) \cdot \mu \cdot \left(\tfrac{\delta}{A_0}\right) - \tfrac{e^{-2K_0}}{2 K_0^2} \left(\tfrac{\delta}{A_0}\right)^2 \} \quad . \end{aligned} \tag{25}$$

Inserting x = Ao into (18) yields the penetration point y (x = A_0) at the exit screen. The independence of the deflection from the site of the shot δ means that $y(x = A_0) \neq f(\delta)$, or $\partial y(x=A_0)/\partial\delta = 0$. Equal coefficients of δ/A_0 in $A_0 \cdot \alpha = f_1(\delta/A_0)$ and $z_2 - z_1 - z_0 = f_2(\delta/A_0)$, then a conditional equation is obtained for K_0. /27

$$\frac{A_0^2}{K_0 \cdot r_0} \cdot \frac{\delta}{A_0} = A_0 K_0 c_0 \, e^{-K_0} \left(\frac{\delta}{A_0}\right) \tag{26}$$

or

$$K_0^2 \, c_0 = 1 \tag{27}$$

$C_0 = C_0 (K_0)$ results from the calculations of

$$J(K,\theta) = J(K_0(1+\mu), \tfrac{\pi}{2} + \alpha) = \int_0^{\pi/2+\alpha} \cos\theta \exp (K_0 \cdot (1+\mu) \cdot \cos\theta) \, d\theta = \tag{28}$$

$$= c_0 + c_{11} \cdot \alpha^2 + c_2 \cdot \mu + c_{22} \cdot \mu^2$$

With $C_0(K_0)\ \text{in}\ (27) : \underline{K_0 = 0{,}7425}\ (\text{and}\ C_0 = 1{,}815)$; (29)

from (21) $\underline{z_0 = A_0 K_0 C_0 = 1{,}35 \cdot A_0}$; (30)

from (13) $z_0 = A_0 \cdot e^{\underline{K_0 = 2{,}1 \cdot A_0}}$. (31)

By maintaining equations (30) and (31), which determine the geometric dimensions of the magnetic pole shoes, the ion beam's exit point y at the exit aperture becomes independent of the shot location.

Equation (28) yields the constants C_0, C_{11}, C_2, C_{22} as functions of K_0. Equation (27) yields

$$C_{11} = -0.5;\ C2 = 1.04;\ C_{22} = 0.356.$$

Entering these values into (18) yields the exit beam equation:

$$y = z_2 - z1 - z_0 - x \cdot \alpha \text{ or,}$$

$$\frac{y}{A_0} = -1{,}56\cdot\theta_1 + 0{,}64\cdot\left(\frac{\delta}{A_0}\right) + 1{,}17\cdot\mu + 0{,}5\cdot\theta_1^2 - 0{,}74\cdot\theta_1\cdot\left(\frac{\delta}{A_0}\right) - 0{,}153\cdot\left(\frac{\delta}{A_0}\right)^2 -$$
$$- 1{,}56\cdot\theta_1\cdot\mu + \mu\cdot\left(\frac{\delta}{A_0}\right) - 0{,}585\cdot\mu + x\cdot\left[-0{,}64\left(\frac{\delta}{A_0}\right) + \mu - 0{,}5\cdot\theta_1^2 + 0{,}153\cdot\left(\frac{\delta}{A_0}\right)^2 + \right.$$
$$\left. + 0{,}64\cdot\mu\cdot\left(\frac{\delta}{A_0}\right) - \mu^2\right] \quad (32)$$

Establishing $x = A_0$ yields the penetration point of the beam at the location of the exit aperture, dependent on the entry parameters.

$$\frac{y}{A_0} = -1{,}56\cdot\theta_1 + 2{,}17\cdot\mu - 0{,}7425\cdot\theta_1\cdot\left(\frac{\delta}{A_0}\right) - 1{,}56\,\theta_1\cdot\mu + 1{,}64\cdot\mu\cdot\left(\frac{\delta}{A_0}\right) - 1{,}525\cdot\mu^2 \quad (33)$$

By varying the parameters δ, θ, μ within the given limits, $y_{max} - y_{min}$ yields beam width b:

$$b = y_{max} - y_{min}$$

The position of the penetration point is not dependent on δ (the location of the shot) in the 1st order, nor on δ^2 in the second order (but certainly from mixed terms).

This fact makes it possible to construct a mass spectrometer whose resolution is independent of the application of an otherwise usual entry aperture. However, the energy and angle deflection of the incoming ion beam must be kept as small as possible (energy homogenous parallel beam).

Determining Dispersion

/28

The y position of the exit beam at the exit aperture ($x = A_0$) should be determined dependent on $\mu = dp/p$ where entry parameters ($\delta = 0$, $\theta_1 = 0$) are fixed.

Equation (34) becomes the following where $p = \sqrt{2e}\, M \cdot U$,

$$\mu = \frac{dp\,(M,U)}{p} = \frac{1}{p}\left[\frac{\partial p(M,U)}{\partial M} \cdot \Delta M + \frac{\partial p(M,U)}{\partial U} \cdot \Delta U\right] \tag{35}$$

(34) becomes:

$$\mu = \frac{1}{2}\,\frac{\Delta M}{M} + \frac{1}{2}\,\frac{\Delta U}{U} \tag{36}$$

Dispersion is derived from equation (36) with (33) and where $\delta = 0$, $\theta_1 = 0$:

$$y = A_0 \cdot 2{,}17 \cdot \frac{1}{2}\left(\frac{\Delta M}{M} + \frac{\Delta U}{U}\right) \tag{37}$$

For $\Delta U = 0$: $y(\Delta M) = 1{,}085 \cdot A_0 \cdot \frac{\Delta M}{M}$ mass dispersion (38)

For $M = 0$: $y(\mu) = 1{,}085 \cdot A_0 \cdot \frac{\Delta U}{U} = 2{,}17 \cdot A_0 \cdot \frac{dp}{p}$ velocity dispersion. (39)

Equation (33) yields beam dispersion $y(\theta_1)$, caused by the angle deflection of the ion beam, where $\mu = \delta = 0$:

$$y(\theta_1) = -1{,}56 \cdot A_0 \cdot \theta_1 \tag{40}$$

Resolution

If the dispersion from (37) is made equal to the sum of the exit aperture and beam dispersion caused by angle deflection $y(\theta_1)$, the following is obtained for resolution A:

$$A = \frac{M}{\Delta M} = \frac{1{,}085 \cdot A_0}{(\Delta U/U + 1{,}44 \cdot \theta_1) \cdot 1{,}085\, A_0 + s_A} \tag{41}$$

The width of the entry aperture is not considered here because the entry opening is theoretically narrowed to 0 during focusing (if $\Delta U = \theta_1 = 0$).

For $s_A = 0$, the theoretical (half-value) resolution is:

$$A_{0,5} = \frac{1}{\Delta U/U + 1{,}44 \cdot \theta_1} \tag{42}$$

To attain a $A_{0,5} = 100$, e.g., the following values must exist: $\Delta U < 1$ V and $\theta_1 < 0.30$. Strict restrictions must therefore be

placed on the beam's parallelism due to the strong dependency of A on angle θ1.

8.2 Technical Appendix

8.2.1. Dual chamber arrangement

The dual chamber principle requires the equipment to have two pump conduits, seen in Fig. 17.

There are three connections between the heating elements in the auxiliary vacuum and the ion source in the main vacuum. They should have a low conductance so that the interaction between heating filaments and the ionization area is largely suppressed.

a) The electron beam is shot into the main chamber through a 1 mm hole which has a molecular conductance of L_E = 0.1 1/sec.

b) The ion beam exits the main chamber through an exit /29
aperture of about 1.3 mm^2 in area (conductance about 0.16 1/sec). Particles which are supposed to travel from the heating filament into the emitter must pass through several corners and narrow areas, however, so that conductance drops to about 0.1 1/sec.

c) For simplicity's sake, the main vacuum chamber and the auxiliary vacuum chamber are evacuated by the same diffusion pump. The two pump connections come together in front of the cooling trap. The conductance from the heating filament to the emitter over this path is about 0.65 1/sec when the valve is completely open; if the valve is opened only one turn of the knob, then conductance drops to about 0.25 1/sec.

8.2.2. Chamber evacuation and the vacuum system

The entire chamber is constructed in steel and can withstand temperatures up to 450°C. The chamber has a volume of about 1 liter. The Conflat-Flanche can be sealed as necessary with viton or copper gaskets.

The evacuation is done with a rotating prepump D2, an oil diffusion pump DO-30 (Leybold) with 35 1/sec suction speed (at 10^{-5} Torr), and a three stage Hickmann glass-oil diffusion pump GF - 25 W with a 25 1/sec suction speed (drive: DC 704).

A glass cooling trap cooled with liquefied air is installed between the pump and the receiver.

A B.A. conduit was used to measure pressure and was placed directly at the entry aperture of the measuring vacuum (ion emitter) to obtain the truest pressure reading. To avoid the conduits influencing the residual gas consistency, it was closed when the spectra were taken.

Targets

The partial pressure measurement was followed by a faraday bowl placed behind the exit aperture of the spectrometer and a screen to suppress secondary electrons. To guarantee good isolation against the housing and to avoid current leakage, the target was installed with a lead to the electrometer at only one location (at the ceramic duct).

Because the magnet pole shoes were permanently installed, the target system was hung to be movable in two directions by means of metal bellows (in the direction of the exit beam and perpendicular to that in the deflector plane). The magnetic field boundary on the exit side was also adjustable during operation, so that the values A_o, z_o, and r_o, determined by the field geometry, (Fig. 16) could be independently varied in order to find the focusing point.

8.2.3. Magnet

A special magnet was developed for this residual gas analyzer and made from armco steel. The entry side of the ion beam can clearly be seen in Fig. 18 with its wedge-shaped pole shoes inclining toward one another. Otherwise, Fig. 18 shows only model pole shoes which are blocked out in order to show the field geometry. The actual pole shoes are welded into the chamber and serve as a chamber wall in the area of the magnet to allow the air gap and thus the dimensions of the magnet to be kept as small as possible. The pole shoes are inclined toward each other at an angle below about 11^0. The pole shoes are about 12 mm apart at the entry aperture and about 5.7 mm apart at the exit aperture.

An A_o of 40 mm was selected, which made possible a central deflector radius of p_m = 46 mm (entry p_E = 62.3; exit p_A = 29.7 mm). The exit aperture is about 40 mm distant from the field boundary.

Theoretically, a round opening could be used as an entry /30 aperture; a short gap was used so as not to complicate the adjustment unnecessarily.

The coils were made of anodized aluminum bands (48 x 0.18 mm cross section). Each coil has about 350 turns. Its resistance was total 0.45 Ohms. During a coil current of 15 A, the magnet at the exit position produced a field of more than 12 KG (Fig. 15).

Because of the relatively large magnet gap, the magnetic dispersion field was covered with [Herzogshunts-could not find: Herzog shunts [38,39]. The dispersion field course was measured with and without cover using an echo sound (Fig. 16). The effective field boundary lay in about the calculated value of 0.4 d in front of the geometric pole shoe edge (d = distance pole shoe screen). The magnetic measurements were appropriately corrected. The parallel displacement of the ion beam by the magnetic dispersal

field was calculated per [28]. It was smaller than 0.1 mm and could be ignored.

The dispersal field at the ion emitter and the electron canon was covered with cylindrical armco screens.

The spectrum (passage of the magnetic field) can be taken by hand or using a synchrometer.

Fig. 15: Strength of the magnetic field as dependent on the coil current

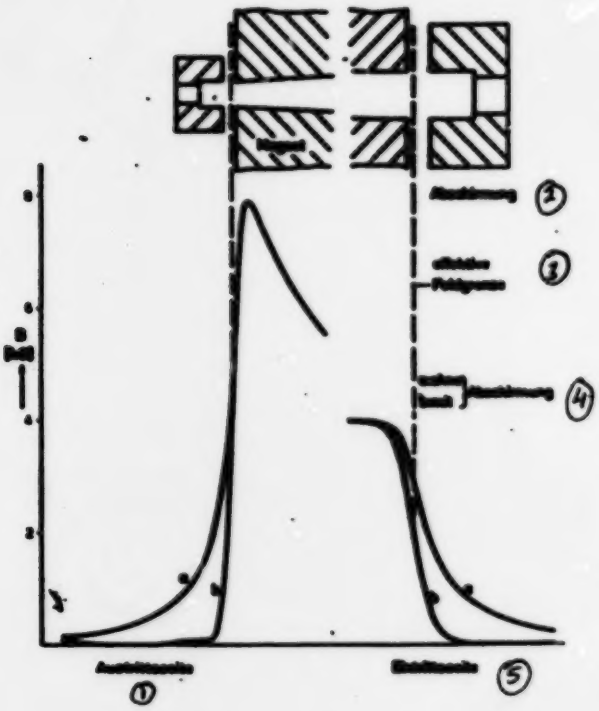

Fig. 16: Course of the dispersion field.

Key: (1) Exit side; (2) Covering; (3) Effective field boundary; (4) a:with, b:without cover; (5) Entry side.

8.2.4. Ion emitter

The ion emitter was mounted on a 2-3/4 inch CF-flange. Fig. 19b shows the coil surrounding the ionization area and the heating filament K_2 for single chamber operation. Excepted is the cylinder surrounding the coil which has large openings for shooting electrons and for evacuation that are covered with highly transparent screens. The uniform field accelerator consists of 2 screen holders (also see Fig. 2) for screens G_1 and G_2 that close off the accelerator area and several interim rings adjusted to one another with glass spheres (tolerance 0.01 mm) to ensure the most exact parallelism of G_1 and G_2. The rings are at equidistant potentials produced by the sequential heating of glass encapsuled, heatable resistors (each 500 kΩ).

The coil was made of 0.3 mm strong chromium nickel wire. Its resistance (30Ω) was measured in such a way that it heats up during operation to 150...250° C.

To equalize the penetration coefficient of the acceleration field in the ionization area, screen G_2 must be at a higher potential than the coil at the screen end. Otherwise, the potential directly surrounding the very thin screen (0.01 .. 0.001 mm) drops sharply, and the area vital for transmission in the center of the mesh has a lower potential than the screen wires. The potentials of screen G_B and of cylinder P can also be established independent of the other tensions. The best results are obtained with the following tensions: /32

U_{Be} = 511 V, U_p = 400 V,
U_{W1} = 500 V,
U_{W2} = 510 V,
U_{GB} = 525 V,
Electron energy U_E = 100 V (re: coil potential)

Screen G_A (90% transmission) past the ion emitter exit serves for total current or total pressure measurement.

Electron canons

The electrons are produced thermally in an auxiliary vacuum chamber far from the measuring area. An electron canon of hairpin cathode, Wehnelt cylinder and single lens [40] shoot an electron beam through screen B into the ion emitter. The single lens permits alteration of the focal distance without changing the energy of the focused electrons. By using diversion plates between the canon and screen B, it was possible to get nearly all (90%) of the electrons emitted by the cathode into the ion source where, due to the potentials in effect, they oscillated across and through the coil where they eventually came to rest. The optimal electron energy was about 100 V.

The current on the coil was used to regulate the thermal efficiency of the cathode by means of a regulating device developed especially for the operation of the canons. This stabilized the emission current very well.

For connection reasons, the emission current was limited to about 110 μA. The current inside the coil sank to 80 μA due to losses during penetration of the screen between the two chambers, the coil and net G_4.

Cathodes were 0.1 strong thoriated wolfram wires. The electron canon was mounted on a 2-3/4 inch Con-Flat-flange and was easily replaceable.

When properly installed, the source delivered a parallel ion beam of almost 10^{-8} A at a pressure of P = 10^{-5} Torr; the sensitivity was therefore E_{Ges} = 10^{-3} A/Torr, or 10 $Torr^{-1}$. This agrees with the theoretically anticipated yield;

$$\varkappa_{ion} = \frac{J^-}{p} = J^- \cdot s \cdot l = 8 \cdot 10^{-3} \frac{A}{Torr}$$

where J^- = 80 μA = electron flow
s = 10 1/Torr cm = differential ionization
l = 1 cm = electron path.

Single chamber operation

To make possible a comparison of the effectiveness of the dual chamber source with a normally operated ion emitter, a second heating filament was installed directly beside the coil. The conductance of this heat filament to the ionization area is very high so that the change in the residual gas composition caused by the heating filament is also evident in the spectrum.

The electron flow and thus the ion flow delivered by the source can be raised during this operation until the volume charge density reaches a limit. From J- = 6 mA (electron flow), the ion flow does not increase as J^- increases. However, it is apparent that ion beam properties (and thus partial pressure resolution and sensitivity) are optimal at J^- = 7.5 mA. /33

To measure the smallest partial pressure (high electron current) while the total pressure in the system is high, the relationship between pressure and ion flow is no longer linear because then the ion flow between the two acceleration nets is limited by the volume charge. The maximal flow between parallel plates is per [41]:

$$J_R = 1{,}71 \cdot 10^{-7} \frac{U_{Be}^{1{,}5} \cdot r^2}{M \cdot d^2} \quad [A]$$

where 2r = beam diameter
d = plate interval
M = ion mass
U_{Be} = acceleration tension

For 2r = 10mm, d = 25 mm, M = 28 and U_{Be} = 500, J_R = 15 μA.

Agreement with the experiment is very good because the strongest current that can be extracted from the emitter was 10 μA (Ar-ions, measured with G_A) at an argon pressure of $3 \cdot 10^{-4}$ Torr.

8.2.5. Photo sensor

To make possible a study of the quality of the ion beam relative to angle deflection, a photo sensor was constructed and functioned as follows:

A filter screen is attached directly at the exit aperture of the ion source. It has 25 holes of 1 mm diameter arranged in a regular geometric pattern at 2 mm intervals. The 25 ion beams penetrate a field-free drift area of about 70 mm to which an angle deflection causes the beams to drift. The beam then falls on a grounded close meshed screen G_{W1} (mesh width 25 μ), optical transmission 48%), is accelerated then to a second negative tension (7.5 kV) net G_{W2} (25 μ, 48%), and there produces secondary electrons. These are partially sucked through lightscreen L (at about 0.5 kV [= ion acceleration energy]) and create a picture of the filter screen that can be observed from the outside through window F. The angle deflection of the total or the individual ion beams can be taken from the picture.

The drift area and the arrangement of the holes were chosen to cause an angle deflection which would make the beam expand sufficiently to permit a comfortable evaluation but still create acceptable resolution.

$A_{0.5} = M/\Delta M = 1/\Delta U/U + 1.44\ \theta_1$ yields, e.g., for $A_{0.5} = 60$, and $\Delta U = 2$ Volt: $\theta_1 = 0.0088 = 0.5^0$.

At 70 mm drift, this means an expansion from 1 mm to 1.63 mm. The individual holes appear separated on the screen.

The photo sensor does not, of course, make a perfect picture. Due to the relatively large middle energy of the secondary electrons (U_e = 2 volt), an infinitely thin ion beam would create an error of δ_B.

[42] yields:

$$\delta_B = 4\,d\sqrt{\frac{U_e}{U_B}} = 0{,}1\ \text{mm}$$

Where U_B = 7 kV = tension between L and G_{W2}.

U_e = 2 volt
d = 1.5 mm = interval L - G_{W2}

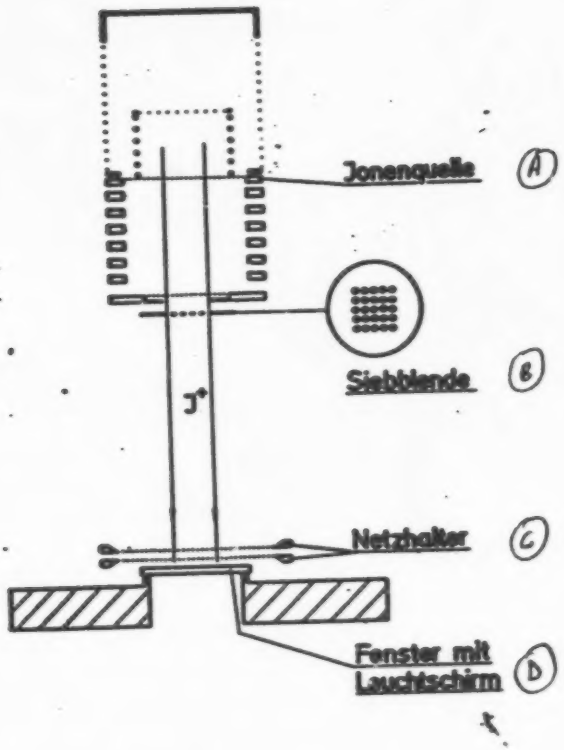

Key: A) - Ion emitter, B) - Screen opening, C) Net support, D) - Window with fluorescent screen

Fig. 20: Photo sensor

ORIGINAL PAGE IS
OF POOR QUALITY

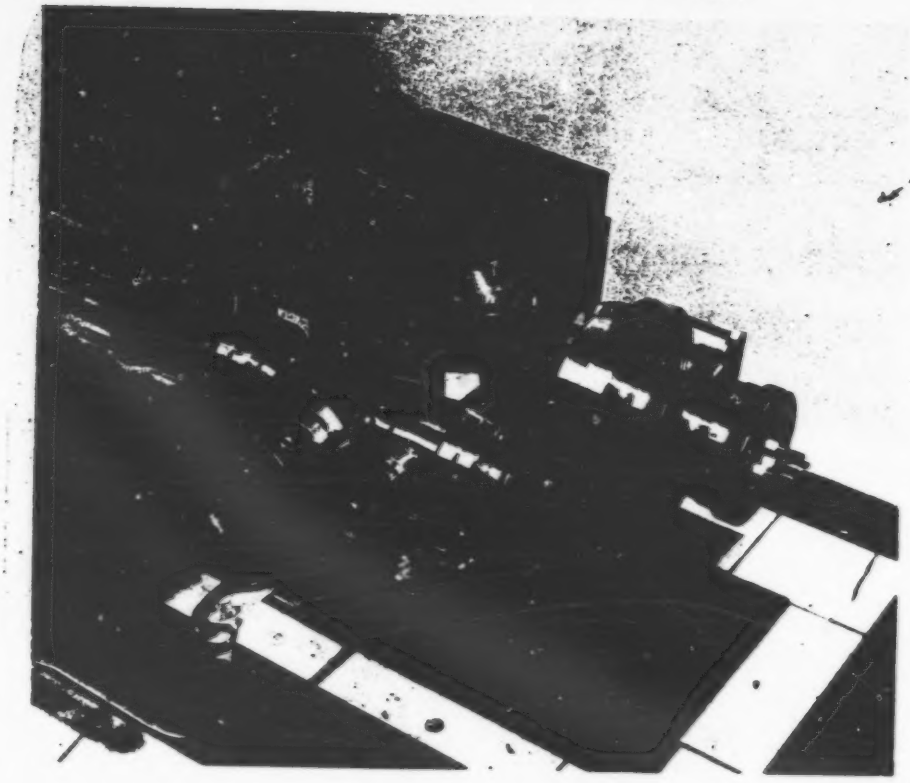

Fig. 17: Full view of the partial pressure analyzer

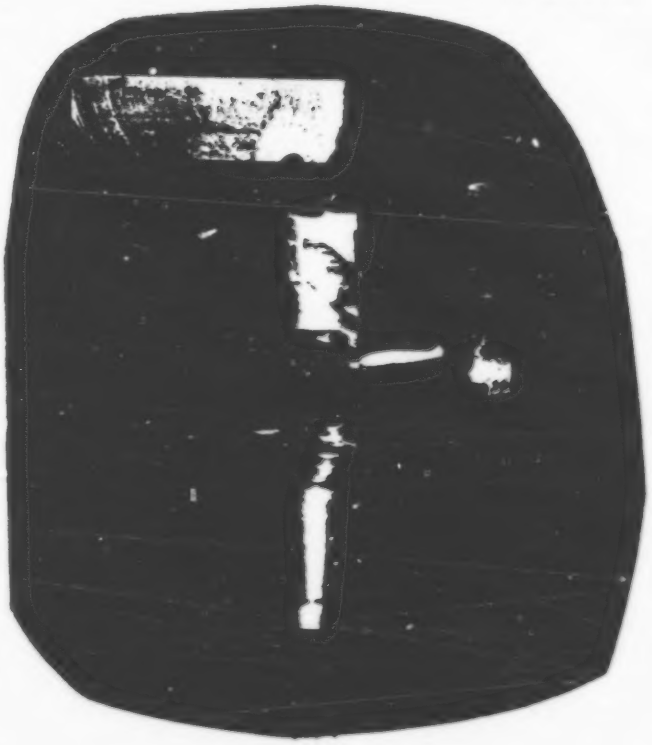

Fig. 18: Magnet

ORIGINAL PAGE IS
OF POOR QUALITY

Fig. 19: A) Ion emitter

Fig. 19: B) Ion emitter disassembled.

BIBLIOGRAPHY

[1] D. Alpert — Le Vide 17 (1962) 19

[2] C.A. Mead — J. Appl.Phys. 32 (1961) 646

[3] M. Alpert — Univ. Illinois CSL Rep. R-286 (1966)

[4] E.E. Windsor — Vac. 20 (1970) 1

[5] J.P. Sprouse, K.E. Jackson, T.A. Raju und H.K. Testermann — 18th Ann.Conf. Mass Spectrometry (1970) California B 281

[6] H.D. Beckey, A. Heinrichs und G. Tenschert — Z. Instr.Kunde 75 (1967) 95

[7] H.K. Testermann et al. — J. Appl.Phys. 36 (1965) 2939

[8] P. Schagen — Brit. J.App.Phys. 16 (1965) 273

[9] F.S. Stein und J.E. Mann — Ortib 58934 (1948) MEDC 1670

[10] W.D. Davis — J. Vac.Sci.Techn. 6 (1969) 85

[11] E.W. Blauth und G. Vonne — Proc. 3rd Int.Vac.Congr. 2 II (1967) 523

[12] E.W. Blauth — Vak.Techn. 17 (1968) 90

[13] H. Ewald und H. Hintenberger — "Methoden und Anwendungen der Massenspektrometrie" (1953)

[14] E.W. Blauth und H. Weissmann — IPP 2/74 (1967)

[15] H.O.W. Richardson — Proc.Phys.Land. 59 (1947) 791

[16] W. Buschbeck und P. Harnack — J.Appl.Phys. 37 (1966) 2812

[17] H. Liebl — J.Appl. 38 (1967) 5277

[18] L.N. Gall, R.N. Gall und N.S. Stepanova — Rev.Phys. T.P. 13 (1968) 790

[19] L.P. Theard — Rev.Sci.Instr. 39 (1968) 1464

[20] G.Strauss — Vac. 20 (1970) 65

[21] H.v. Ardenne — "Tabellen d. Elektronenphysik, Ionenphysik und Übermikroskopie" I (1956) 50

[22] P.A. Redhead und J.P. Hobson — Phil.Trans.Roy. Land. A 251 (1968) 35

[23]	P.A. Redhead	14th ASTM Ann.Conf. Mass Spectrometry Dallas, Texas
[24]	J. Cuthbert et al.	Proc.Phys.Soc. 88 (1966) 91
[25]	K.R. Ryan und J.H. Futrell	12th ASTM Ann.Conf. Mass Spectrometry Montreal, Kanada
[26]	D. Kuppke	Handbuch d. Phys. Bd. 33 (1956) 38
[27]	H. Rothe und W. Kleen	"Hochvakuumelektronenröhren" (1955)
[28]	P.A. Redhead I.P. Robson und E.V. Kornelsen	The physical basis of UHV (1968) 275
[29]	L.N. Gill und N.K. Vasil'eva	Sov.Phys.-T.P. 10 (1966) 1149
[30]	N.J. Freeman und N.R. Daly	J.Sci.Instr. 44 (1967) 956
[31]	N.J. Freeman N.R. Daly und R.E. Powell	Rev.Sci.Instr. 38 (1967) 965
[32]	K.A. Kaiser und C.M. Stevens	ANL 7393 (1967)
[33]	R.E. Fox und J.A. Hipple	Rev.Sci.Instr. 19 (1948) 462
[34]	T.W. Hickmott	J.Chem.Phys. 32 (1960) 840
[35]	J.H. Singleton	J.Vac.Sci. and Techn. 4 (1967) 103
[36]	H.W. Robinson	"The physical principles of UHV systems and equipment" (1968) 150
[37]	P.A. Redhead	J.Vac.Sci.Techn. 7 (1970) 182
[38]	R.F.K. Herzog	Z. Naturforschung 10a (1955) 887
[39]	L.A. König und F. Hintenberger	Z. Naturforschung 10a (1955) 887
[40]	E.W. Mauth	"Dynamische Massenspektrometer" (1965)
[41]	O.R. Morgan G.S. Kelley und R.C. Davis	Rev.Sci.Instr. 38 (1967) 467
[42]	M.v. Ardenne	"Tabellen der Elektronenphysik, Ionenphysik und Übermikroskopie" I (1956) 516
[43]	H. Liebl	unveröffentlicht
[44]	W.R. Smythe L.H. Rumbaugh und S.S. West	Phys.Rev. 45 (1968) 722

[45] H.J. Hintemann — Proc. 4th Int.Vac.Congr. (1968) 722

[46] J.H. Reynolds — Rev.Sci.Instr. 27 (1956) 928

[47] S. Garke — Vak.Techn. 12 (1962) 201

[48] W.D. Davis — Trans AVS Vac.Symp 9 (1962) 363

[49] J.L. Robins — Can.J.Phy. 41 (1963) 1585

[50] P.A. Redhead — Can.J.Phy. 42 (1964) 886

[51] P. Marmet und J.D. Morrison — J.Chem. Phy. 36 (1962) 1238

[52] R.H. Plumbee und L.P. Smith — J.Appl.Phy. 21 (1950) 811

[53] D. Lichtmann — J.Vac.Sci. Techn. 2 (1965) 70

[54] G.E. Moore und P.C. Unterwald — J.Chem.Phys. 40 (1964) 2626

[55] W.K. Huber und G. Rettinghaus — J.Vac.Sci.Techn. 6 (1969) 89

[56] W.K. Huber und G. Rettinghaus — J.Vac.Sci.Techn. 7 (1970) 289

[57] J.W. Coburn — Surf.Sci. 11 (1968) 61

[58] M.J. Batsiev und M.J. Jonov — Sov.Phys.-T.P. 12 (1968) 821

[59] A.J.R. Robertson — Adv. in Mascpectr. (1959) 559

[60] wie [13] S. 68